PCCP

ROYAL SOCIETY OF CHEMISTRY

PAPER

View Article Online
View Journal | View Issue

Cite this: *Phys. Chem. Chem. Phys.*, 2025, **27**, 17930

Comparison of the solvation models COSMO and EC-RISM for the prediction of photoacidity in aqueous solution

Ömer F. C. Tiska, [a] Niklas Sülzner, [a] Julia Haberhauer, [a] Patrick Kibies, [b] Stefan M. Kast [b] and Christof Hättig *[a]

The embedded cluster reference interaction site model (EC-RISM) and the conductor-like solvation model (COSMO) are compared in terms of their ability to predict excitation energies and photoacidity in aqueous solution. The test set includes photoacids derived from phenol, naphthol, and coumarin as well as photobases derived from quinoline. Vertical excitation energies were calculated using the approximate coupled cluster singles-and-doubles model (CC2). For the neutral and protonated forms of the photobases as well as for the neutral forms of the photoacids, EC-RISM-CC2 and COSMO-CC2 yield excitation energies that agree within approximately ±0.08 eV and are in good agreement with available experimental data. For the deprotonated forms of the photoacids, which in this study are phenolate anions throughout, COSMO significantly underestimates the effects of hydrogen bond donation in aqueous solution. In contrast, EC-RISM provides a more faithful description of these solvation effects due to its ability to model solvent distributions on an atomic level, unlike continuum approaches such as COSMO. As a result, EC-RISM performs better in predicting the photoacidity of the photoacids while yielding similar results for the photobasicity of the photobases. To approximately correct for the remaining electronic structure error of CC2, higher-order corrections were estimated from vacuum calculations with CCSDR(3) and CC3 and added to the EC-RISM-CC2 results. For the excitation energies of the photoacids, the CCSDR(3) and CC3 results exhibit significant differences, with the CC3 corrections leading to better agreement with the available experimental data in solution. However, regarding photoacidity, the estimated EC-RISM-CCSDR(3) and EC-RISM-CC3 results are very similar.

Received 5th May 2025,
Accepted 30th July 2025

DOI: 10.1039/d5cp01694k

rsc.li/pccp

1 Introduction

Proton transfer is one of the most fundamental reactions in both nature and the laboratory.[1–3] The ability to induce a proton transfer with a laser pulse can be crucial for synthetic purposes such as photoinduced polymerization[4,5] or for mechanistic studies.[6–12] To achieve a controlled proton transfer, different classes of photoacids and photobases are used.[4–11] Photoacids are molecules that exhibit increased acidity after photoexcitation to higher electronic states (*e.g.*, see ref. 13 for a recent review). However, the conjugated bases formed after such an excited-state proton transfers (ESPT) are not photobases; rather, they exhibit the opposite behavior: a decrease in basicity. Photobases, by definition, are molecules that, analogously to the photoacids, exhibit an increase in basicity upon excitation.[14–18]

Unlike in the ground state, the lifetime of excited states is too short to allow for direct measurement of the equilibrium constant K_a^* for the proton transfer in the excited state.[19] Therefore, it has to be determined using alternative methods. A quantitative description of photoacidity was first introduced by Förster, who proposed a thermodynamic cycle[20,21] that links ground-state acidity to acidity in the excited state. According to the Förster cycle, the increase in acidity upon excitation (ΔpK_a^*) is obtained from the difference of the (standard) Gibbs energies of excitation between the acid $\Delta G_{exc}(HA)$ and the base $\Delta G_{exc}(A^-)$ through

$$\Delta pK_a^* = pK_a^* - pK_a = \frac{\Delta G_{exc}(A^-) - \Delta G_{exc}(HA)}{RT \ln 10} \quad (1)$$

with R as the molar gas constant and T as the absolute temperature. $\Delta G_{exc}(X)$ is the difference between the Gibbs energy of X in the excited state, $G^*(X)$, and in the ground state, $G(X)$, in solution including full solvent relaxation also in the excited state.

[a] *Lehrstuhl für Theoretische Chemie, Ruhr-Universität Bochum, 44780 Bochum, Germany. E-mail: christof.haettig@rub.de; Tel: +49 (0)234 32 28082*
[b] *Fakultät für Chemie und Chemische Biologie, Technische Universität Dortmund, Otto-Hahn-Str. 4a, 44227 Dortmund, Germany. E-mail: stefan.kast@tu-dortmund.de*

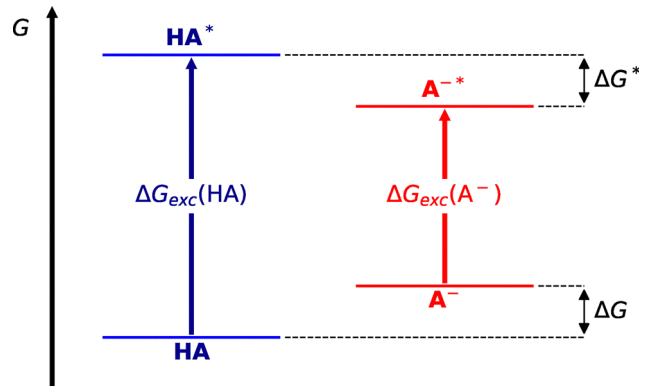

Fig. 1 Schematic representation of the Förster cycle showing the relation of the excitation Gibbs energies of the acid (blue) and the conjugated base (red) to the change in the reaction Gibbs energy for the proton transfer from the ground to the excited state (marked with *).

As shown in Fig. 1, the Förster cycle replaces the Gibbs energy difference in the excited state (ΔG^*) by the ground-state value (ΔG) and the difference in the excitation Gibbs energies for HA and A^-. In spectroscopic studies, the latter are usually approximated by 0–0 transition energies.[19] This implies the approximation of $\Delta G_{exc}(X)$ by excitation energies, $\Delta E_{exc}(X)$. In practice, excitation energies in solution are often determined as band maxima which correspond for isolated bands to the vibronic transitions with the largest Franck–Condon factor. In computational studies, excitations are typically treated as vertical transitions from the minimum of the initial state without including vibrational contributions and under the assumption of a "frozen" solvation structure. These are also not directly related to the 0–0 transition energies. Nevertheless, it has been shown for both experimental band maxima as well as computed vertical transition energies that the average of absorption and emission provides a good approximation of the 0–0 transition energies due to compensation effects.[22,23]

Alternatively, photoacidity can also be determined through kinetic measurements of ESPT.[24–27] However, this approach is experimentally challenging and applicable to only a few molecules for which ESPT dynamics can be measured.[19] Therefore, the most common method for determining excited-state acidity is *via* the Föster cycle.[19]

Due to the sensitivity of the acidity increase ΔpK_a^* to solvation effects, the photoacidity can be used in theoretical chemistry as a criterion for the accuracy of solvation models.[28–30] As many relevant chemical reactions occur in the condensed phase, the importance to give an accurate description of solvent effects becomes more and more evident.[31,32] It is also apparent that a full quantum-mechanical description of solute and solvent *e.g.* by *ab initio* molecular dynamics simulations is computationally demanding and in practice realizable at the DFT level only,[33] while so-called machine learning potentials will perspectively allow for higher-level treatment of solvated ensembles when they are trained against, *e.g.*, post-Hartree–Fock reference data. Therefore, the task of describing the solvent becomes a question of compromising the quality of the method and computational power.

Besides explicitly including the solvent together with the solute at an atomistic level in the computational model, there are also alternative options to approximate solvent effects. One important approach is to consider the solvent as a polarizable continuum which implicitly accounts for averaging over the thermal motions of solvent molecules.[34–36] Due to the implicit nature, computations with such models are far less demanding than with explicit solvation. This idea provides the basis for the whole class of continuum solvation models (CSMs).[34–36] One widespread class of CSMs are apparent surface models (ASMs), to which the conductor-like screening model[37] (COSMO) belongs. ASMs approximate the surrounding charge distribution by projecting it on the apparent surface of a cavity around the molecule.

An alternative to ASMs are solvation models based on atomistic solvent site distributions such as the embedded cluster reference interactive site model (EC-RISM). They retain the idea of implicit models to include in the electronic structure calculation for the solute a solvent-exhibited electrostatic potential averaged over the thermal motions of the solvent molecules, thereby, preserving the computational efficiency of implicit models. The reference interaction site model (RISM)[38–40] or more specifically the three dimensional version 3D RISM[41–43] is based on approximating the molecular Ornstein–Zernicke equations using solvent orientation averaging while preserving the 3D molecular solute structure, yielding site distribution functions of the solvent molecules around the solute by employing a suitable closure relation.[44] Hence, 3D RISM captures the granularity and internal structure of the solvent without the need of explicit simulation. In EC-RISM this approach is coupled to the quantum-mechanical calculation of the solute's electronic structure, where the solvent-exhibited potential is approximated by embedding the solute in point charges that are derived from the solvent site distribution functions, which are computed self-consistently with the solute's wave function.[45] EC-RISM has found numerous applications to the prediction of NMR- and EPR-spectroscopic parameters as well as thermodynamic problems, see ref. 46–50 for a selection. Readers are referred to the reviews for a broader overview of RISM-derived solvation models in the context of electronic structure calculations.[51,52]

In a previous publication, the deficiency of COSMO in accurately describing the photoacidity of phenols in water was demonstrated.[53] More precisely, it was shown that the solvent effects on the excitation energies of their conjugated bases are poorly modeled. This was traced back to an insufficient description of hydrogen bonding, which resulted from the simplicity of ASMs. Unlike COSMO, EC-RISM accounts for the internal structure of the solvent and is therefore better able to mimic specific solvent–solute interactions, such as hydrogen bonding.

In this work, we evaluate EC-RISM's ability to describe solvation effects on excitation energies in aqueous solution. As a test set we use oxygen-based photoacids (phenol, naphthol and coumarin derivatives) and nitrogen-based photobases (quinoline derivatives). The acid and base forms of these molecules differ in the number of hydrogen bonds they donate or accept, thus providing a challenging test for modelling the effects of hydrogen bonding on excitation energies. The approximate coupled cluster

singles-and-doubles model[54] CC2 is used as electronic structure method. Results are compared with experimental data and those obtained with COSMO. To estimate the magnitude of the remaining errors from CC2 as electronic structure method, vacuum-based corrections from higher-order coupled-cluster methods with approximate iterative connected triples[55] (CC3) and a perturbative triples correction[56] (CCSDR(3)) are employed.

2 Computational details

2.1 General information

All calculations have been performed with a development version based on release V7.8 of the TURBOMOLE program package.[57,58] The Hartree–Fock calculations were done with the dscf[59] module. The RI approximation was used in all CC2, CCSDR(3), and CC3 calculations. These were done with the ricc2[60] and ccsdf12 modules, and the frozen-core approximation was applied to the 1s orbitals at C, N, and O, the 1s2s2p orbitals at Cl, and the 1s2s2p3s3p orbitals at Br. The test set of molecules was taken from ref. 53. To account for solvation effects, the solvation models COSMO[37] and EC-RISM[45] were used. These calculations were done for aqueous solutions.

For COSMO, this was realized by choosing a dielectric constant of $\varepsilon = 78.30$ and a refractive index of $n = 1.30$ as used in ref. 53. For smooth potential energy surfaces with COSMO, the Gaussian charge model (GCM) was employed with default parameters for the cavity construction.[61]

For EC-RISM, the distribution of the solvent was evaluated at $T = 298.15$ K and $p = 1$ bar with a solvent density of 0.03332950 Å^{-3} and dielectric constant of $\varepsilon = 78.447$ using the modified SPC/E water model employed earlier[49,62] 78.447 is the experimental value for ε at 1 bar and 298.15 K, for which this specific water model was defined for ref. 49 and 62. For 3D RISM calculations the PSE-1 closure[44] was employed. For a numerically stable treatment of electrostatic potential a switching scheme was applied. In the direct vicinity of the solute the electrostatic potential is used on a grid (*vide infra*) as calculated from the solute's orbital-relaxed CC2 ground-state charge density, while in a buffer zone beginning at the perimeter of a sphere with a radius 1 Å smaller than the inscribed sphere of the calculation box a cubic interpolation function is used to switch to the ESP calculated from atomic partial charges to obtain the latter at and outside the inscribed sphere.[63]

The 3D RISM calculations were performed on a cubic grid with 128 lattice points along each principal axis and a spacing of 0.3 Å. The convergence criteria were set to 10^{-6} for the maximum residual of the direct correlation functions within the 3D RISM calculations and to an SCF convergency criterion of 10^{-7} a.u. and a density convergence criterion of 10^{-6} a.u. Auxiliary atom-centered point charges were calculated using the Merz–Kollman scheme with standard radii. Lennard-Jones parameters for the photoacids were determined using Antechamber 22 with GAFF 1.81.[64–66]

2.2 Geometry optimization in solution

The geometries were optimized for the ground state at the CC2 level[54] using COSMO with the post-SCF[67] reaction field coupling scheme.[34] For this, the def-TZVP orbital and auxiliary basis sets[68–70] were used. For tightly converged structures, the threshold for the cartesian gradient was set to 10^{-4} a.u. For cases where the orientation of the O–H group results in distinguishable conformers, geometry optimizations yielded two structures differing at most by 5 kJ mol^{-1}. Only the lower-energy conformers were considered, as the differences in the excitation energies between the conformers—a mean absolute deviation of 0.02 eV—were found to be negligible. The main difference from the computational protocol used for geometry optimizations in ref. 53 lies in the GCM employed for COSMO.

2.3 Excitation energies in solution

The excitation energies were calculated for the structures optimized at the COSMO-CC2 level using both COSMO and EC-RISM as solvation models. Excitations up to the second $\pi \rightarrow \pi^*$ transition were calculated. For this, the def2-TZVPPD orbital and auxiliary basis sets[71,72] were used. The reaction field scheme was changed from the post-SCF to the more complete perturbation with self-consistent energy and density (PTED) scheme with and without linear response contributions.[36,73,74] In the PTED calculations, the reaction field was self-consistently equilibrated with the orbital-relaxed CC2 ground-state charge density. No non-equilibrium corrections are included. Since the EC-RISM implementation only includes the static polarizability of the solvent due to the specification of a force field-based unpolarizable water model, the linear response contributions to excitation energies could not be taken into account by this solvent model. To correct for this, we added to the EC-RISM results the differences between excitation energies obtained from PTED-COSMO calculations with and without response contribution, as proposed in ref. 75. These results are denoted in the following as EC-RISM(+LR). Note that the COSMO results for excitation energies reported below always include the response contribution.

2.4 Higher-method corrections

To evaluate the residual errors from CC2 as electronic structure method, calculations with the higher-order methods[55,56] CCSDR(3) and CC3 were performed. These are approximations to CCSDT with $\mathcal{O}(\mathcal{N}^7)$-scaling computational costs. Both give excitation energies for single excitation dominated transitions that are correct to third order in the fluctuation potential. CC3 keeps the iterative character of CCSDT, while CCSDR(3) adds a non-iterative perturbative correction to the CCSD results. Since these methods are not yet available in combination with COSMO or EC-RISM, the comparison was conducted *in vacuo*. For consistency, the structures were reoptimized *in vacuo* using CC2 with the def2-TZVPPD basis sets, employing C_s symmetry (C_{2v} for phenolate). For these structures the excitation energies were then calculated with CC2, CCSDR(3), and CC3 with the same basis. The differences in the excitation energies between CC2 and these higher-order methods were subsequently added to the EC-RISM(+LR)-CC2 values. In the following, these results are referred to as est. EC-RISM(+LR)-CCSDR(3) and est. EC-RISM(+LR)-CC3, respectively.

2.5 Acidity change upon excitation

The acidity changes upon excitation from the ground to the excited state have been calculated as:

$$\Delta \mathrm{p}K_\mathrm{a}^* = \mathrm{p}K_\mathrm{a}^* - \mathrm{p}K_\mathrm{a} = \frac{\Delta E_\mathrm{exc}(\mathrm{A}^-) - \Delta E_\mathrm{exc}(\mathrm{HA})}{RT \ln 10} \quad (2)$$

where $\Delta E_\mathrm{exc}(\mathrm{X})$ are the vertical excitation energies for X. The states chosen for the calculation of $\Delta \mathrm{p}K_\mathrm{a}^*$ are marked in Tables 1 and 5. We evaluated the $\mathrm{p}K_\mathrm{a}$ change for T = 298.15 K with R = 8.314 J mol^{-1} K^{-1} and 1/(RT·ln 10) = 16.9044 eV^{-1}. To analyse the correlation between calculated acidity changes, $\Delta \mathrm{p}K_\mathrm{a}^*$ (calc.), and experimentally determined acidity changes, $\Delta \mathrm{p}K_\mathrm{a}^*$(exp.), we fitted to the results the linear relation:

$$\Delta \mathrm{p}K_\mathrm{a}^*(\mathrm{exp.}) = c_0 + \Delta \mathrm{p}K_\mathrm{a}^*(\mathrm{calc.}) \cdot c_1 \quad (3)$$

using least squares regression.

3 Results and discussion

3.1 Photoacids

3.1.1 Excitation energy calculations in solution. In Table 1, we listed the calculated excitation energies at the CC2 level for the lowest two $\pi \rightarrow \pi^*$ transitions for both the neutral and deprotonated species. By natural transition orbital (NTO) analysis, the transitions were assigned according to the Platt notation[91] to either $^1\mathrm{L_a}$ or $^1\mathrm{L_b}$ and compared to the respective experimental band maxima where available. Fig. 2 shows a statistical evaluation of the differences between excitation energies obtained with COSMO and EC-RISM (Fig. 2(a)) and the deviations from the experimental band maxima (Fig. 2(b)) as box plots.

COSMO and EC-RISM yield similar results for the neutral species of the photoacids. Without adding the COSMO-based linear-response corrections, the excitation energies differ on average by 33 meV, with the $^1\mathrm{L_a}$ states exhibiting slighthly larger differences than the $^1\mathrm{L_b}$ states. The largest deviation between COSMO and EC-RISM is found for the $^1\mathrm{L_a}$ state of phenol, where the difference amounts to 86 meV. Once the response contributions are included, the EC-RISM results agree with those from COSMO within 42 meV, though the average difference, due to compensation effects, is only 2 meV. Whether with or without response contributions, the differences between the two solvation models are below 100 meV. To set this in perspective, it should be compared with the typical residual error of 100–200 meV of CC2 excitation energies for valence transitions in organic molecules.[83,84] As seen in Fig. 2(b), the COSMO-CC2 results for vertical excitation energies for absorption overestimate the experimental band maxima on average by 332 meV. The use of EC-RISM slightly increases the overestimation to 372 meV (no response) and 335 meV (with response). Compared to the absolute mean deviations of the computed from the experimental results, it is fair to say that EC-RISM and COSMO perform similarly for the neutral forms of the photoacids.

Unlike for the neutral species, the results for the deprotonated forms show a stronger dependence on the solvation model. Instead of a few meV, the difference between the results obtained with COSMO and EC-RISM amounts on average to 295 meV (no response) and 250 meV (with response). In all cases where experimental data was found, the COSMO results for the vertical excitation energies underestimate the experimental band maxima. The underestimation ranges from 33 meV to 403 meV with an average value of 187 meV. This contradicts the experience that vertical transition energies are usually $\approx 0.1 \pm 0.1$ eV blue shifted relative to the band maxima.[83,84] A red shift of this magnitude suggests that major contributions to the solvent effects for the deprotonated species in aqueous solution are not accounted for by COSMO as already noted in ref. 53. Contrary to COSMO, the EC-RISM solvation model leads for the same transitions to excitation energies that are blue shifted relative to the experimental band maxima. The pure EC-RISM even pushes all the excitations over the edge to a blue shift. Only when adding the response contribution of COSMO, the results for two molecules are slightly red shifted compared to the band maxima (see Fig. 2). Unlike for COSMO, the red shifts obtained with EC-RISM are less pronounced, reaching at most $\approx$30 meV. The exact cause of these red shifts remains unclear. One possibility is that EC-RISM still underestimates the effects of hydrogen bonding for phenolate anions due to the approximate closure relation. Alternatively, a residual electronic structure error may be responsible (*vide infra*). Another potential explanation is that the usual relationship between vertical excitation and band maximum does not hold in these cases due to the overlap with the band of a nearby state.

When the response contribution is not added, the excitation energies for the deprotonated species of the photobases are on average blue shifted by 142 meV. With the response contribution included, the average blue shift is reduced to 85 meV.

In ref. 53, COSMO-CC2 cluster-continuum calculations were conducted with the post-SCF reaction field scheme for the phenol–phenolate acid–base pair to investigate the stability of the results upon including explicit solvent molecules. One explicit water molecule was included for phenol and three for phenolate. For the current work, we repeated the cluster-continuum calculations with PTED-COSMO-CC2 and PTED-EC-RISM-CC2 using the optimized geometries from ref. 53. To disentangle direct solvent effects caused by explicit water molecules from indirect effects due to changes in the solute geometry, we also performed PTED calculations with only the solute but using the structure optimized in cluster-continuum calculations (Table 2). For the neutral species (phenol), the results from the cluster-continuum calculation are red-shifted by only 0.07 eV relative to the pure COSMO result, with about one third of this difference arising from the geometry change. The respective EC-RISM calculations yield excitation energies that are consistently $\approx$30–40 meV higher. This fits to the above finding that EC-RISM gives for the neutral forms of the photoacids results close to those obtained with COSMO, in most cases slightly blue-shifted.

In contrast to phenol, including explicit water molecules in the COSMO calculations for the phenolate anion leads to a significant blue shift of 0.33 eV, although the change in the geometry of the solute alone causes a red shift of 0.06 eV. With

Table 1 Character of the lowest two $\pi \rightarrow \pi^*$ transitions for the neutral and deprotonated forms of the photoacids and comparison of the calculated vertical CC2 excitation energies with experimentally determined band maxima (in eV). The listed oscillator strengths were calculated with COSMO-CC2. The states used to calculate the acidity change upon excitation are highlighted in bold font

Compound	Character	COSMO	EC-RISM	EC-RISM(+LR)	Oscillator strength	Experiment
1-Naphthol	^1L_b	4.29	4.32	4.31	0.027	3.86[a]
	$^1\mathbf{L_a}$	4.44	4.50	4.46	0.120	4.25[b]
5-Cyano-1-naphthol	$^1\mathbf{L_a}$	3.89	3.92	3.89	0.139	—
	^1L_b	4.20	4.21	4.20	0.007	—
5-*tert*-Butyl-1-naphthol	^1L_b	4.21	4.24	4.23	0.031	—
	$^1\mathbf{L_a}$	4.32	4.39	4.35	0.161	4.19[c]
2-Naphthol	$^1\mathbf{L_b}$	4.20	4.22	4.22	0.028	3.79[a]
	^1L_a	4.80	4.81	4.81	0.041	—
5-Cyano-2-naphthol	$^1\mathbf{L_a}$	3.98	4.01	3.98	0.075	3.68[d]
	^1L_b	4.40	4.42	4.39	0.083	—
Phenol	$^1\mathbf{L_b}$	4.94	4.99	4.97	0.032	4.59[e]
	^1L_a	6.09	6.17	6.13	0.116	—
2-Cyano-phenol	$^1\mathbf{L_b}$	4.58	4.61	4.58	0.086	4.15[f]
	^1L_a	5.77	5.82	5.77	0.140	5.32[f]
3-Cyano-phenol	$^1\mathbf{L_b}$	4.58	4.61	4.58	0.066	4.23[f]
	^1L_a	5.69	5.73	5.69	0.122	5.28[f]
4-Cyano-phenol	$^1\mathbf{L_b}$	4.88	4.90	4.89	0.008	4.43[f]
	^1L_a	5.37	5.43	5.36	0.492	5.05[f]
3-Hydroxycoumarin	$^1\mathbf{L_a}$	4.22	4.26	4.20	0.379	4.04[g]
	^1L_b	4.64	4.64	4.62	0.082	—
7-Hydroxycoumarin	$^1\mathbf{L_a}$	4.12	4.16	4.09	0.420	3.81[h]
	^1L_b	4.59	4.59	4.57	0.048	—
7-Hydroxy-4-methylcoumarin	$^1\mathbf{L_a}$	4.15	4.19	4.13	0.388	3.87[h]
	^1L_b	4.66	4.65	4.64	0.065	—
1-Naphtholate	$^1\mathbf{L_a}$	3.44	3.82	3.79	0.112	3.72[a]
	^1L_b	3.78	4.03	4.00	0.126	—
5-Cyano-1-naphtholate	$^1\mathbf{L_a}$	2.78	3.13	3.10	0.104	—
	^1L_b	3.70	3.94	3.91	0.108	—
5-*tert*-Butyl-1-naphtholate	$^1\mathbf{L_a}$	3.41	3.78	3.74	0.155	3.72[c]
	^1L_b	3.75	4.00	3.97	0.117	—
2-Naphtholate	$^1\mathbf{L_b}$	3.36	3.73	3.70	0.083	3.61[a]
	^1L_a	4.32	4.55	4.52	0.198	—
5-Cyano-2-naphtholate	$^1\mathbf{L_a}$	2.94	3.34	3.31	0.095	3.34[d]
	^1L_b	4.01	4.21	4.19	0.061	—
Phenolate	$^1\mathbf{L_b}$	4.13	4.53	4.49	0.066	4.33[e]
	^1L_a	5.00	5.48	5.40	0.308	—
2-Cyano-phenolate	$^1\mathbf{L_b}$	3.73	4.03	3.98	0.146	3.79[f]
	^1L_a	5.09	5.36	5.29	0.183	5.12[f]
3-Cyano-phenolate	$^1\mathbf{L_b}$	3.63	4.02	3.98	0.084	3.79[f]
	^1L_a	4.84	5.20	5.14	0.211	5.06[f]
4-Cyano-phenolate	$^1\mathbf{L_b}$	4.25	4.55	4.52	0.052	—
	^1L_a	4.45	4.73	4.63	0.657	4.53[f]
3-Hydroxycoumarin (−1)	$^1\mathbf{L_a}$	3.58	3.83	3.75	0.416	3.78[g]
	^1L_b	4.23	4.47	4.45	0.011	—
7-Hydroxycoumarin (−1)	$^1\mathbf{L_a}$	3.29	3.53	3.45	0.537	3.40[h]
	^1L_b	4.23	4.37	4.35	0.049	—
7-Hydroxy-4-methylcoumarin (−1)	$^1\mathbf{L_a}$	3.32	3.58	3.50	0.503	3.44[h]
	^1L_b	4.25	4.40	4.37	0.046	—

[a] Taken from ref. 76. [b] Taken from ref. 19. [c] Taken from ref. 77. [d] Taken from ref. 78. [e] Taken from ref. 79. [f] Taken from ref. 80. [g] Taken from ref. 81. [h] Taken from ref. 82.

the EC-RISM solvation model, the PTED result with the solute alone is already close to the COSMO cluster-continuum result. The change of the geometry alone leads also with EC-RISM to a red-shift of 0.06 eV. Unlike COSMO, including the water molecules in the excitation energy calculation results in only a small blue shift, which is only marginally larger than the red shift caused by the geometry change. Consequently, the EC-RISM cluster-continuum result differs by just 0.01 eV from the EC-RISM result for the solute alone, demonstrating the stability of the EC-RISM calculations upon the inclusion of explicit solvent molecules. The difference between the excitation energies for the protonated and deprotonated forms, which determines the acidity change upon excitation, is the same within 0.01 eV for the cluster-continuum results obtained with COSMO and with EC-RISM.

3.1.2 Higher-order correlation corrections. Fig. 3 shows a comparison of the deviation of the est. EC-RISM(+LR)-CCSDR(3), est. EC-RISM(+LR)-CC3, and EC-RISM(+LR)-CC2 excitation energies from the experimental band maxima for the states used to calculate ΔpK_a^*. A statistical summary of the higher-order correlation corrections from CCSDR(3) and CC3 for all studied states of the photoacids and their conjugated bases is given in Fig. 4.

In most cases, CCSDR(3) predicts higher excitation energies than CC2, exceptions are mainly the ^1L_b states of the phenols and the 1-naphthols. Unlike CCSDR(3), CC3 gives in most cases

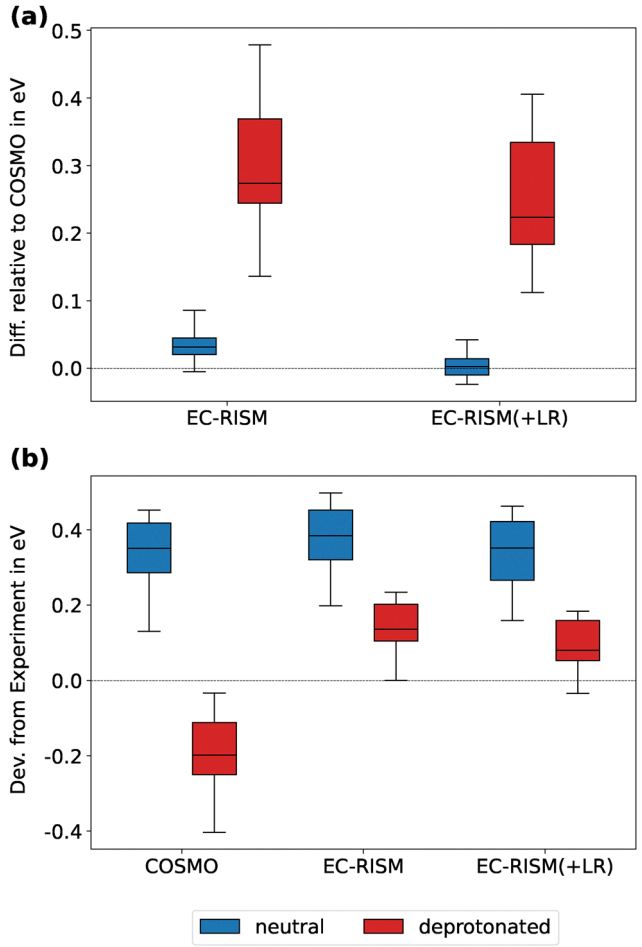

Fig. 2 Vertical excitation energies for photoacids in their neutral and deprotonated form: (a) difference between CC2 excitation energies obtained with EC-RISM or EC-RISM(+LR) and those obtained with COSMO for all states. (b) Deviation between computed and experimental absorption energies for all states were experimental data was found.

Table 2 Comparison of the excitation energy (eV) for the phenol–phenolate (PhOH–PhO$^-$) system obtained with COSMO-CC2 and EC-RISM(+LR)-CC2 as well as with the respective cluster-continuum approach including for PhOH one and for PhO$^-$ three explicit water molecules

	COSMO			EC-RISM(+LR)			
Compound	PTED	PTED[a]	Clust. cont.[b]	PTED	PTED[a]	Clust. cont.[b]	Exp.[c]
PhOH	4.94	4.92	4.87	4.97	4.95	4.91	4.59
PhO$^-$	4.13	4.06	4.46	4.49	4.43	4.50	4.33
$\Delta_{\mathrm{PhOH-PhO^-}}$	0.81	0.86	0.41	0.48	0.54	0.41	0.26

[a] Calculated with cluster-continuum structure excluding explicit water molecules. [b] Calculated with the PTED reaction field scheme. [c] Taken from ref. 79.

negative corrections to the excitation energies. Both align with the usual trends observed for valence transitions in organic molecules,[85,86] although the deviations between the CCSDR(3) and the CC3 results for the photoacids are at the upper end of the range typically observed for the lowest valence transitions when dominated by single excitations.

For the neutral acid species, the higher-order corrections alter the excitation energies by up to $\approx\pm0.2$ eV. On average, CCSDR(3) increases the results 43 meV, while CC3 decreases them by 40 meV (see Fig. 3). Except for 5-cyano-2-naphthol, the CC3 corrections are larger for ^1L_b than for ^1L_a. 5-Cyano-1-naphthol is also the only exception in our test set of photoacids where the CC3 higher-order correction is slightly positive for ^1L_b.

Adding the CC3 correction to the PTED(+LR)-EC-RISM-CC2 results leads for the neutral photoacids in most cases to a better or an only slightly worse agreement the experiment. CCSDR(3), however, improves the agreement of the computed excitation energies with the experimental band maxima only for the phenols. On average, CC3 reduces the deviation from the available experimental data from 335 meV (for CC2) to 288 meV, CCSDR(3) slightly raises it to 366 meV. We note, however, that in particular in aqueous solution vertical excitation energies can deviate from band maxima by 200–300 meV.[87] Thus, the comparison with the experimental band maxima can only serve as a qualitative measure for the accuracy of the computed vertical excitation energies.

For the deprotonated species, the corrections from CCSDR(3) are in all cases positive, on average 107 meV. CC3, on the other hand, sometimes yiels negative corrections, particularly for the coumarins. In comparison to CCSDR(3), the corrections from CC3, are, with a mean absolute value of only 31 meV, again smaller. With the CCSDR(3) corrections, the average deviation of the computed excitation energies from the experimental band maxima is with 190 meV about twice as large as for EC-RISM-CC2. With the CC3 corrections the average deviation is with 92 meV only slightly larger than for EC-RISM-CC2. In many cases, the CC3-corrected results are close to those from EC-RISM-CC2.

3.1.3 Changes in acidity upon excitation. In Table 3, the results for the acidity change upon excitation, ΔpK_a^*, are listed. As mentioned above, the deficiencies of COSMO lead to a significant underestimation of the excitation energies for the deprotonated species of the photoacids. This results in a substantial underestimation of ΔpK_a^* by PTED-COSMO-CC2, on average by about 8.2 pK_a units. Changing the solvation model from COSMO to EC-RISM reduces this underestimation on average by 5 pK_a units, leading to an improvement for all molecules. This change appears to be uniform for both the naphthols and the phenols. The coumarins, on the other hand, experience relatively small changes, on average 3.3 pK_a units. For most of the molecules, the inclusion of the response contributions leads to a slight increase in excited-state acidity. However, for 1-naphthol and its derivatives, the excited-state acidity decreases when linear response contributions are included.

Even though CCSDR(3) and CC3 deviate significantly for the excitation energies, the resulting changes in ΔpK_a^* are very similar. For many molecules, the higher order corrections improve agreement with experimental data. In particular, for 2-naphthol and 5-cyano-2-naphthol, where the EC-RISM-CC2 results for ΔpK_a^* still deviated by more than 5 pK_a units from the experimental values, the corrections from CCSDR(3) and

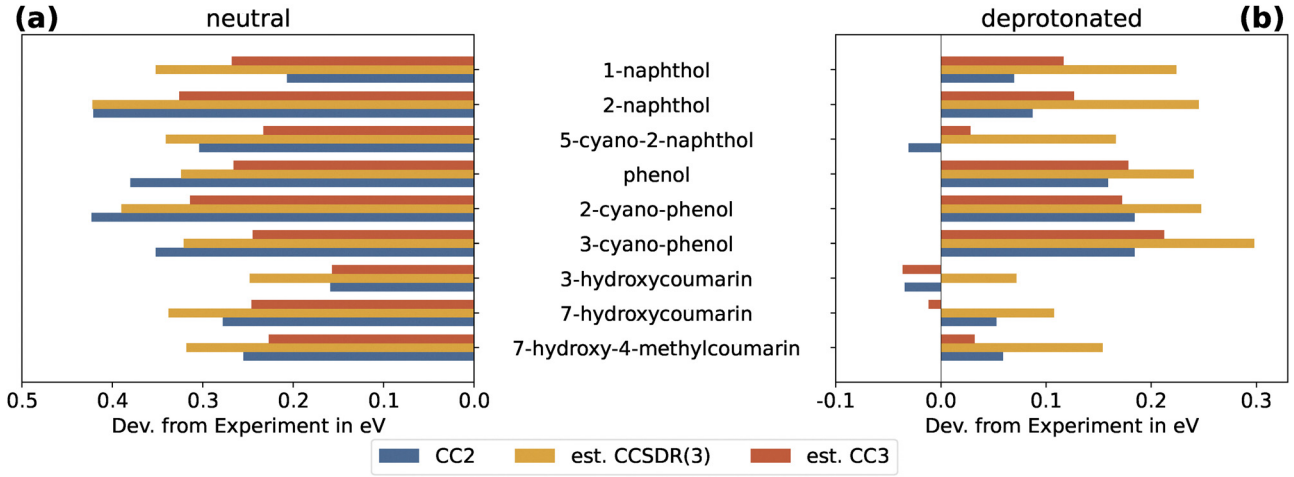

Fig. 3 Deviation of the EC-RISM(+LR) vertical excitation energies of lowest $^1\pi\pi^*$ for the neutral (a) and the deprotonated (b) species of the photoacids from experimental data for the states used to calculate ΔpK_a^*. The excitation energy of CC2 as well as those including CCSDR(3) and CC3 corrections are shown.

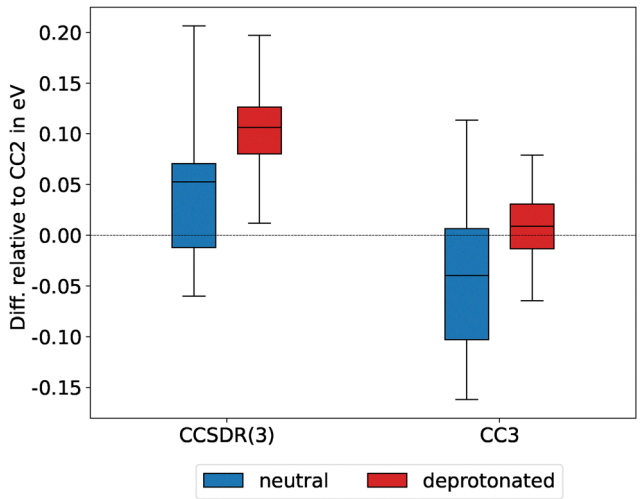

Fig. 4 Higher-order corrections obtained with CCSDR(3) and CC3 for the neutral and the deprotonated species of the photoacids.

CC3 reduce these deviations, bringing them more in line with those for other molecules. For 1-naphthol, 5-cyano-1-naphthol, and 7-hydroxycoumarin, the corrections result in an increased deviation of approximately 0.5 pK_a units. The phenols perform extraordinarily well, deviating on average by only a single pK_a unit from the experimental values. Even though, on average, the higher-order method corrections lead to an improvement of 1 pK_a unit, this improvement in the current test set mainly affects those photoacids that have a small ΔpK_a^* (*cf.* Fig. 5).

To identify systematic errors and distinguish them from non-systematic errors, we performed a linear regression (*cf.* eqn (3)). The results are summarized in Table 4. Fig. 5 shows the data points in scatter plots, where the errors of the computed values correspond to the horizontal distances of the points from the diagonal lines which represent perfect agreement with experiment. Systematic errors become mainly noticeable through deviations of the regression lines's slope and intercept from the ideal values 0 and 1, respectively.

As expected, the results of this analysis confirm the previously discussed underestimation of ΔpK_a^* by COSMO: the regression line is significantly shifted to the left. This shift arises from the insufficient description of hydrogen bonding, which causes a large red shift in the excitation energies of the deprotonated forms. EC-RISM-CC2, both with and without response contributions, yields better results, as indicated by slopes close to 1. Moreover, for EC-RISM the regression lines have higher coefficients of determination (R^2) suggesting smaller non-systematic errors. Depending on whether response contributions are included, the intercept for EC-RISM-CC2 is either similar to or slightly smaller than for COSMO-CC2. For the results including higher-order corrections from CCSDR(3) and CC3, the R^2 values are even highger—0.82 for CCSDR(3) and 0.79 for CC3. In this test set, the higher correlation corrections lead in particular for systems with small ΔpK_a^* values to results that closely match experimental photoacidities. However, for large ΔpK_a^*, they do not improve upon the CC2 results. This behaviour is reflected in a low intercept near 0, but a slope similar to that of COSMO.

3.2 Photobases

3.2.1 Excitation energy calculations in solution. In Table 5, the excitation energies of the neutral and protonated forms of the photobases are listed. Again, the lowest two $^1\pi\pi^*$ states can in most cases be characterized according to the Platt notation[91] as either ^1L_a or ^1L_b based on the NTOs. For acridine, quinoline, and the 5-substituted quinolines, our calculations show that the positions of the ^1L_b states are almost unaffected by protonation, with shifts between +60 and −60 meV, whereas the ^1L_a states shift substantially to the red, by −350 meV to −750 meV. Only for 6-methoxyquinoline both of the lowest two $\pi \rightarrow \pi^*$ transitions do shift in the calculations by −320 meV to −470 meV upon protonation. This is mostly in line with

Table 3 Change in acidity ΔpK_a^* obtained for the photoacids with vertical excitation energies from COSMO-CC2, EC-RISM-CC2, and estimated EC-RISM-CCSDR(3) and EC-RISM-CC3 results in comparison with experimental values. For the computed excitation energies the PTED coupling scheme was used

	CC2			est. CCSDR(3)	est. CC3	Experiment	
Compound	COSMO	EC-RISM	EC-RISM(+LR)	EC-RISM(+LR)	EC-RISM(+LR)	Absorption[a]	Förster[b]
1-Naphthol	−16.81	−11.38	−11.30	−11.13	−11.53	−8.97	−8.7[d]
5-Cyano-1-naphthol	−18.85	−13.43	−13.34	−14.10	−14.57	−11.3[b]	−11.3
5-*tert*-Butyl-1-naphthol	−15.38	−10.28	−10.24	−10.44	−10.60[f]	−7.87	−8.8
2-Naphthol	−14.22	−8.24	−8.80	−6.14	−6.52	−3.14	−6.5[d]
5-Cyano-2-naphthol	−17.53	−11.25	−11.35	−8.65	−9.17	−5.70	−10.0[e]
Phenol	−13.65	−7.70	−8.03	−5.70	−5.78	−4.30	−7.0
2-Cyano-phenol	−14.44	−9.78	−10.11	−8.49	−8.48	−6.08	−7.5
3-Cyano-phenol	−16.02	−9.89	−10.17	−7.72	−7.89	−7.34	−7.3
4-Cyano-phenol	−10.53	−5.97	−6.33	−4.05	−4.05	−4.41[c]	−4.5
3-Hydroxycoumarin	−10.80	−7.31	−7.65	−7.35	−7.64	−4.37	−4.4
7-Hydroxycoumarin	−14.05	−10.55	−10.88	−10.96	−11.42	−7.07	−6.5[e]
7-Hydroxy-4-methylcoumarin	−14.05	−10.29	−10.58	−10.06	−10.57	−7.28	−6.9

[a] *Via* Förster cycle with absorption energies taken from Table 1. [b] Förster cycle results from the compilation in ref. 53, if not noted otherwise, using the average of absorption and emission band maxima. [c] From kinetic measurements. Taken from ref. 80. [d] Only from absorption band maxima. [e] Only from emission band maxima. [f] Estimation with a restricted virtual space (*cf.* SI).

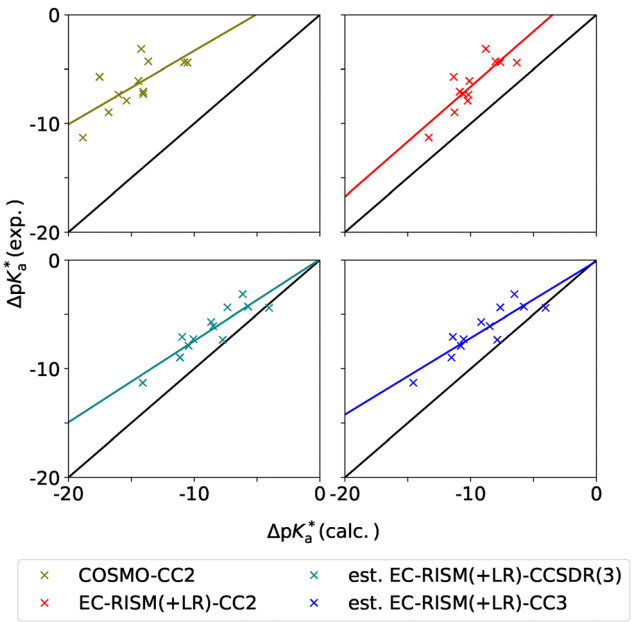

Fig. 5 Correlation plots with experimental ΔpK_a^* (absorption) for the photoacids with the respective linear regression following the eqn (3). The plots for COSMO (green), EC-RISM (orange), CCSDR(3) (teal) and CC3 (blue) are given. In each plot the black line indicates a perfect correlation.

Table 4 Results for the linear regression analysis with experimental ΔpK_a^* (absorption) for the photoacids. The coefficient of determination (R^2), the slope, and the interecept are listed. The errors of the slope and interecept are given in terms of 1σ

Method	R^2	Slope	Intercept
COSMO-CC2	0.52	0.68 ± 0.21	3.45 ± 3.05
EC-RISM-CC2	0.74	0.97 ± 0.18	2.88 ± 1.78
EC-RISM(+LR)-CC2	0.70	1.01 ± 0.21	3.54 ± 2.10
est. EC-RISM(+LR)-CCSDR(3)	0.82	0.75 ± 0.11	0.07 ± 1.02
est. EC-RISM(+LR)-CC3	0.79	0.71 ± 0.12	−0.10 ± 1.14

experimental observations, although the experimentally observed shifts for the ^1L_b transitions are a somewhat larger, particularly for quinoline and 5-cyanoquinoline, where they amount to −230 meV and −360 meV, respectively.

For the photoacids, the insufficient description of hydrogen bonding by COSMO led for the deprotonated forms to large errors in the excitation energies, resulting in significant changes when the solvation model is altered to EC-RISM. In contrast, for the photobases, we find only moderate changes from COSMO to EC-RISM for both the protonated and neutral forms. In Fig. 6(a) the difference of EC-RISM-CC2 and EC-RISM(+LR)-CC2 relative to COSMO-CC2 is shown in form of box plots. The differences are on the order of only a few 10 meV with only small variations from one molecule to another. In particular, the changes are roughly the same for both forms of the photobases. Photobasicity results from the difference of the excitation energies between the base and its conjugated acid. If both forms are affected the same by changing the solvation model to EC-RISM, ΔpK_a^* remains unaffected. On average, the excitation energies change from COSMO-CC2 to EC-RISM-CC2 by only 19 meV for the neutral and by 23 meV for the protonated species. With added response contributions, the changes amount only to −5 meV for the neutral and to −2 meV for the protonated species. The largest changes for pure EC-RISM are observed for the ^1L_a states of 5-cyanoquinoline, 6-methoxyquinoline, and the protonated form of the latter. For both, EC-RISM gives vertical excitation energies that are ≈50 meV higher. Most of this blue shift is, however, due the missing linear response contribution. For EC-RISM(+LR), the largest changes are only ≈−28 meV and were found for the ^1L_a states of quinoline and 5-methoxyquinoline.

A comparison with the experimental data shows that the computed results align for neutral species slightly better with experimental band maxima than for the protonated forms (see Fig. 6(b)). On average, the results for the neutral species deviate from the experimental data with COSMO by 163 meV and with EC-RISM(+LR) by 157 meV. The scattering around the average

Table 5 Character of the lowest two $\pi \rightarrow \pi^*$ transitions for the neutral and protonated forms of the photobases and comparison of the calculated vertical CC2 excitation energies with the experimentally determined band maxima (in eV). The listed oscillator strength were calculated with COSMO-CC2. The states used to calculate the acidity change upon excitation are highlighted in bold font

Compound	Character	COSMO	EC-RISM	EC-RISM(+LR)	Oscillator strength	Experiment
Acridine	$^1\mathbf{L_a}$	3.59	3.62	3.58	0.08	3.54[a]
	^1L_b	3.87	3.89	3.87	0.07	3.51[a]
Quinoline	^1L_b	4.43	4.45	4.43	0.04	4.21[b]
	$^1\mathbf{L_a}$	4.71	4.72	4.68	0.08	4.48[b]
5-Cyanoquinoline	^1L_b	4.33	4.35	4.33	0.08	4.24[b]
	$^1\mathbf{L_a}$	4.64	4.69	4.64	0.18	4.42[b]
5-Chloroquinoline	^1L_b	4.36	4.38	4.36	0.03	4.08[b]
	$^1\mathbf{L_a}$	4.52	4.53	4.50	0.10	4.26[b]
5-Bromoquinoline	^1L_b	4.36	4.39	4.38	0.03	4.09[b]
	$^1\mathbf{L_a}$	4.49	4.52	4.49	0.11	4.24[b]
5-Methoxyquinoline	$^1\mathbf{L_a}$	4.11	4.11	4.09	0.10	4.01[b]
	^1L_b	4.33	4.35	4.34	0.00	—
6-Methoxyquinoline	$^1\mathbf{L_a}$	3.96	4.00	3.97	0.09	3.82[c]
	Mixed	4.58	4.59	4.57	0.02	4.57[c]
Acridinium	$^1\mathbf{L_a}$	3.24	3.26	3.23	0.05	3.22[a]
	^1L_b	3.85	3.88	3.85	0.25	3.50[a]
Quinolinium	$^1\mathbf{L_a}$	4.13	4.14	4.12	0.06	4.05[b]
	^1L_b	4.39	4.41	4.39	0.09	3.98[b]
5-Cyanoquinolinium	$^1\mathbf{L_a}$	4.20	4.23	4.19	0.15	4.01[b]
	^1L_b	4.38	4.41	4.38	0.08	3.88[b]
5-Chloroquinolinium	$^1\mathbf{L_a}$	3.90	3.91	3.88	0.08	3.85[b]
	^1L_b	4.33	4.35	4.33	0.06	3.93[b]
5-Bromoquinolinium	$^1\mathbf{L_a}$	3.87	3.87	3.85	0.08	3.83[b]
	^1L_b	4.32	4.34	4.32	0.06	3.93[b]
5-Methoxyquinolinium	$^1\mathbf{L_a}$	3.38	3.41	3.39	0.08	3.39[b]
	^1L_b	4.28	4.30	4.28	0.00	—
6-Methoxyquinolinium	$^1\mathbf{L_a}$	3.48	3.53	3.51	0.09	3.68[c]
	Mixed	4.25	4.28	4.25	0.05	3.96[c]

[a] Determined from spectra in ref. 88. [b] Determined from spectra in ref. 89. [c] Taken from ref. 90, order of states reassigned.

deviation is for all solvation models similar with a standard deviation (1σ) of $\approx$110 meV. For the protonated species, this deviation is increased to 194 meV with COSMO and to 191 meV with EC-RISM(+LR). Additionally, the scattering of all solvation models is also increased relative to the scattering for the neutral species to $\approx$210 meV, showing a slight tendency of a worse comparability for the protonated form. Despite that, the difference remains marginal in comparison with the deviations from experiment. The vertical excitation energies obtained at the CC2 level are only for the ^1L_a state of the 6-methoxyquinolinium cation significantly red-shifted relative to the experimental band maximum, by 200–150 meV, depending on the solvation model. This is mostly due to higher-order correlation effects not accounted for in CC2 (*vide infra*). Because of the lack of data, the band maxima had to be determined by hand. In these cases, the spectra were also more complex which made it difficult to assign the band maxima. This might be the reason why the computed excitation energies agree for these cases less good with the band maxima from the experimental spectra than for the rest of the molecules.

3.2.2 Higher-order correlation corrections. The system size for the quinoline photobases and acridine is on average subtantially larger than for the photoacids studied above. To mitigate the computational bottleneck that arises with the larger system sizes in the higher-order coupled cluster calculations, the restricted virtual space (RVS) approximation[92] was used in some of the CC3 calculations. For further details we refer to the SI.

For the photobases, the higher-order method corrections from CCSDR(3) and CC3 are larger than the changes from COSMO to EC-RISM (*cf.* Fig. 6 and 7), especially if the response contributions are included with EC-RISM(+LR). Depending on the molecule, the corrections from CCSDR(3) and CC3 vary between −154 meV and +220 meV. This can also be seen in Fig. 7 which shows a statistical evaluation of the higher-order corrections from CCSDR(3) and CC3 for the neutral and protonated forms of the photobases. The scattering, reflected in the plot by the lengths of the boxes, is for both CCSDR(3) and CC3 and for the neutral and protonated forms roughly equal and amounts to $\approx$100–150 meV. For CCSDR(3), the correction is on average +57 meV for the neutral photobases and +48 meV for the protonated forms. Whereas CCSDR(3) gives mainly a positive correction, CC3 shows the opposite behaviour.

Similar as the shifts upon protonation, also the higher-order corrections exhibit different trends for the ^1L_a and ^1L_b transitions in acridine, quinoline, and the 5-substituted quinolines: for ^1L_a the corrections are positive—the only exception is with −10 meV the CC3-corrections for the quinolinium cation—and for ^1L_b they are always negative.

The CCSDR(3) corrections worsen the agreement between the computed vertical excitation energies and the experimental band maxima for the photobases. The mean absolute deviations increase from CC2 to CCSDR(3) for the neutral photobases from 157 meV to 221 meV and for the protonated species from 218 meV to 243 meV. With the CC3 corrections, the

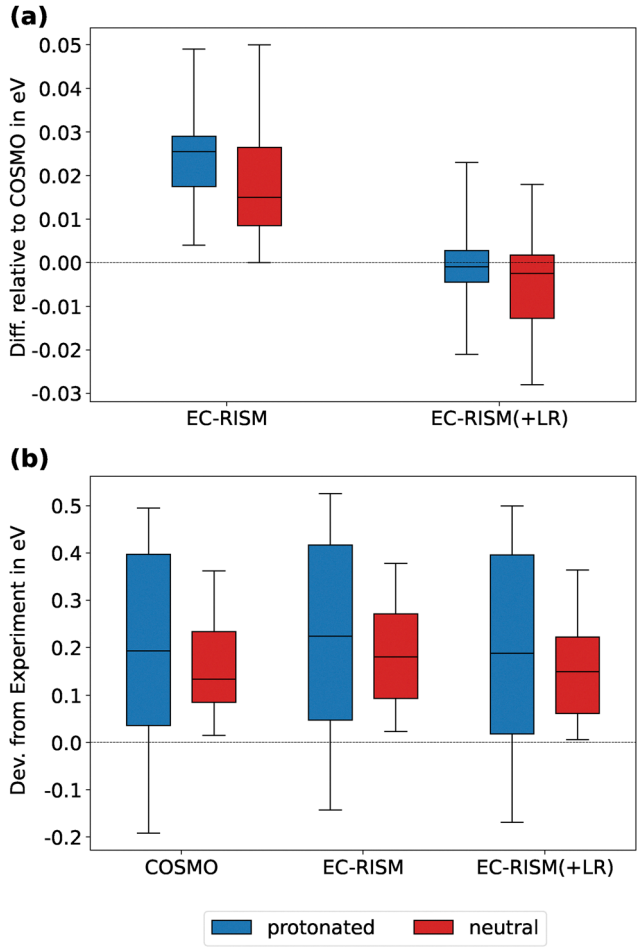

Fig. 6 Vertical excitation energies for photobases in their neutral and protonated form: (a) difference between CC2 excitation energies obtained with EC-RISM or EC-RISM(+LR) and those obtained with COSMO for all states. (b) Deviation between computed and experimental absorption energies for all states where experimental data was found.

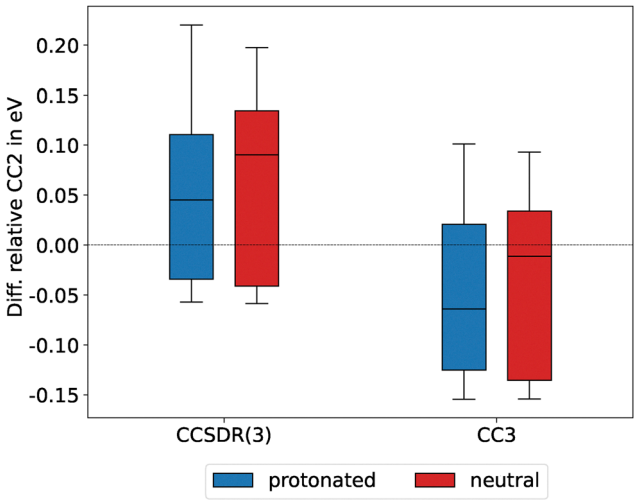

Fig. 7 Correction with CCSDR(3) and CC3 for the neutral and the protonated species of the photobases.

average deviation is decreased to 118 meV for the neutral and to 139 meV for the protonated species. A slightly higher deviation for the protonated species remains for results with both corrections.

3.2.3 Changes in acidity upon excitation. Table 6 lists the results for the acidity change upon excitation, ΔpK_a^*, for the photobases. A statistical evaluation of the deviations between results from computed excitation energies from those obtained with the experimental absorption band maxima is given in Table 7.

In Section 3.2.1 we found that the COSMO and the EC-RISM solvation models give for both the neutral and protonated forms of the photobases similar results for the excitation energies. In line with this, also the results for ΔpK_a^* obtained with the two solvation models at the CC2 level are similar. Unlike for the photoacids, the acidity change of the photobases is already described relatively well with COSMO. The mean square deviation (MSD) from the experimental data is with COSMO 3.41 pK_a units if compared with reference values obtained from experimentally estimated 0-0 transition energies and 2.46 pK_a units if compared with reference values from obtained experimental absorption band maxima. Similar small are the differences between the pure EC-RISM-CC2 and the EC-RISM(+LR)-CC2 results.

More substantial are the effects of the higher-order correlation corrections on ΔpK_a^*. The MSD from the reference values obtained from the absorption band maxima decreases for the results obtained with the estimated EC-RISM(+LR)-CCSDR(3) excitation energies to 2.03 pK_a units and with the estimated EC-RISM(+LR)-CC3 results to 2.15 pK_a units. For most photobases, the higher-order corrections are in the order of a few tenth of a pK_a unit. Exceptionally large corrections of 0.70 with CCSDR(3) and 0.84 with CC3 are found for 5-methoxyquinoline and, even more strikingly, of −2.18 with CCSDR(3) and −1.94 with CC3 for 6-methoxyquinoline. As above for the photoacids, the corrections to ΔpK_a^* from CCSDR(3) and CC3 are very similar. For the photobases, they differ in most cases by less than 0.25 pK_a units. An exception is 5-cyanoquinoline where CCSDR(3) gives a correction of 0.44 and CC3 a correction of 0.92 pK_a units.

The results of the correlation analysis for the changes in acidity for the photobases obtained with the reference values from the experimental absorption band maxima are shown in Table 8 and Fig. 8. COSMO-CC2 and EC-RISM-CC2 give already a reasonable good correlation with the experimental data, although R^2 is only around 0.6. The low R^2 is mostly a consequence of the outlying value for ΔpK_a^* for 6-methoxyquinoline, which deviates for the CC2 results by about 5.5 pK_a units from the experimental reference value. For COSMO, the linear regression yields a slope of 1.03 and an intercept of −2.02 pK_a units. For EC-RISM without response contribution, the slope and the intercept deviate with, respectively, 1.11 and −2.81 pK_a units slightly more from the ideal values of 1 and 0. When the response contributions are included, the slope and intercept are with 1.08 and −2.39 pK_a units close to the values obtained for the COSMO results.

The higher-order correlation contributions from CCSDR(3) and CC3 shift ΔpK_a^* for the outlier 6-methoxyquinoline closer to

Table 6 Change in acidity ΔpK_a^* obtained for the photobases with vertical excitation energies from COSMO-CC2, EC-RISM-CC2, and estimated EC-RISM-CCSDR(3) and EC-RISM-CC3 results in comparison with experimental values. For the computed excitation energies the PTED coupling scheme was used

	CC2			est. CCSDR(3)	est. CC3	Experiment	
Compound	COSMO	EC-RISM	EC-RISM(+LR)	EC-RISM(+LR)	EC-RISM(+LR)	Absorption	0-0 transition
Acridine	6.03	6.02	5.84	6.71	6.73	7.08[a]	4.73[b]
Quinoline	9.79	9.70	9.56	10.10	10.16	7.10[a]	6.70[c]
5-Cyanoquinoline	7.46	7.78	7.56	8.00	8.48	6.99[c]	2.20[c]
5-Chloroquinoline	10.44	10.50	10.39	10.87	10.92	9.85[a]	5.90[c]
5-Bromoquinoline	10.61	11.00	10.89	11.38	11.47	10.25[a]	6.70[c]
5-Methoxyquinoline	12.36	11.94	11.85	12.55	12.57	10.44[a]	10.20[c]
6-Methoxyquinoline	7.99	7.94	7.89	5.71	5.92	2.49[a]	6.60[c]

[a] Determined *via* Förster cycle with absorption energies taken from Table 5. [b] Determined *via* Förster cycle with 0–0 transition energies. Taken from ref. 88. [c] Determined *via* Förster cycle with average of absorption and emission energies. Taken from ref. 93.

Table 7 Statistical evaluation of the deviations between ΔpK_a^* obtained for the photobases from computed vertical excitation energies and experimental absorption band maxima

Method	MSD	Median	Max	Min
COSMO-CC2	2.46	0.59	5.51	0.36
EC-RISM-CC2	2.41	0.79	5.45	0.55
EC-RISM(+LR)-CC2	2.34	0.63	5.40	0.37
est. EC-RISM(+LR)-CCSDR(3)	2.03	1.24	3.23	1.01
est. EC-RISM(+LR)-CC3	2.14	1.49	3.44	1.07

Table 8 Results for the linear regression analysis with experimental ΔpK_a^* (absorption) for the photobases. The coefficient of determination (R^2), the slope, and the interecept are listed. The errors of the slope and interecept are given in terms of 1σ

Method	R^2	Slope	Intercept
COSMO-CC2	0.59	1.03 ± 0.39	-2.02 ± 3.67
EC-RISM-CC2	0.64	1.11 ± 0.38	-2.81 ± 3.56
EC-RISM(+LR)-CC2	0.62	1.08 ± 0.38	-2.39 ± 3.56
est. EC-RISM(+LR)-CCSDR(3)	0.90	1.08 ± 0.16	-2.61 ± 1.58
est. EC-RISM(+LR)-CC3	0.90	1.12 ± 0.17	-3.06 ± 1.66

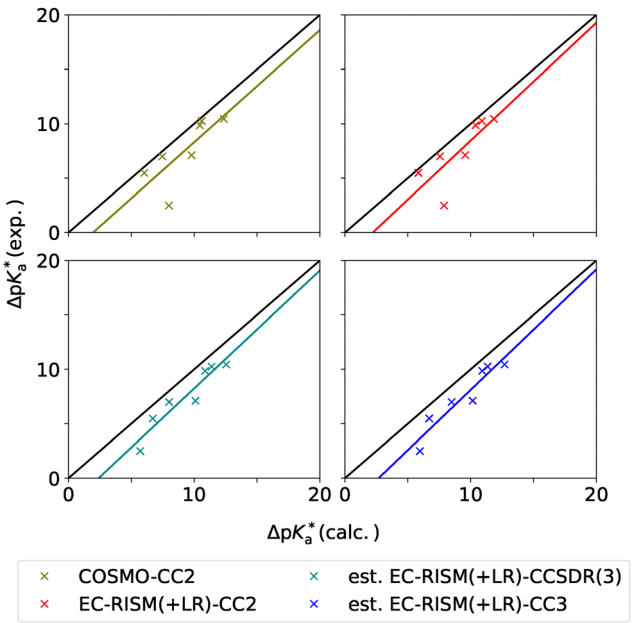

Fig. 8 Correlation plots with experimental ΔpK_a^* (absorption) for the photobases with the respective linear regression following the eqn (3). The plots for COSMO (green), EC-RISM (orange), CCSDR(3) (teal) and CC3 (blue) are given. In each plot the black line indicates a perfect correlation.

the experimental value and the regression line. As a consequence, the coefficient of determination increases to 0.90 for CCSDR(3) and CC3, which is slightly larger than the R^2 values obtained with these methods for the photoacids. For the estimated EC-RISM(+LR)-CCSDR(3) results the intercept is lowered to -2.61 pK_a units while the slope remains 1.08. Similarly, for the estimated EC-RISM(+LR)-CC3 results the slope is 1.12 and the intercepts -3.06 pK_a units.

4. Conclusions

In this work, the capabilities and limitations of the solvent model EC-RISM in describing the acidity change upon excitation, ΔpK_a^*, of photoacids and photobases in aqueous solution has been studied and compared with the apparent surface model COSMO. For this, we used CC2 as electronic structure method and the PTED reaction field coupling scheme. To account for the excitonic coupling or linear response contribution to excitation energies, which can currently not be described with EC-RISM due to missing parameterizations for the solvent's polarizability at optical frequencies, we took this contribution from COSMO calculations. Despite the conceptual differences between the two solvent models COSMO and EC-RISM, they yield similar results for excitation energies in aqueous solution as long as hydrogen bonding effects are not too large. However, for phenolate anions in aqueous solution, COSMO gives poor results for the excitation energies that are substantially less accurate than for the neutral phenols due to the insufficient description of the specific solvent effects from hydrogen bonds between solute and solvent. EC-RISM describes these strong solvent effects much better than COSMO.

For the acidity change upon excitation, ΔpK_a^*, the unbalanced results obtained with COSMO for neutral phenols and the corresponding phenolate anions leads to large errors. COSMO typically overestimates for oxygen-based photoacids

the acidity increase from the ground to the excited state by more than 5 pK_a units compared to experimental values. The improved description of the solvent's potential around the solute provided by EC-RISM largely reduces these errors. A correlation analysis for computed and experimental results for ΔpK_a^* reveals that EC-RISM reduces for the oxygen-based photoacids the systematic shifts as well as the scattering in the deviations between the experimental and the computed results. For the N-heterocyclic aromatic photobases, hydrogen-bonding between solute and solvent has apparently only small effects on the lowest excitation energies and EC-RISM and COSMO perform similar well for the excitation energies and ΔpK_a^*.

Higher-order correlation effects estimated by CCSDR(3) and CC3 calculations change the results for ΔpK_a^* by up to almost 3 pK_a units. In most cases, the higher-order corrections for ΔpK_a^* are positive, but there are also exceptions like 5-cyano-1-naphthol and 6-methoxyquinoline. Despite the fact that CCSDR(3) and CC3 predict excitations energies that differ by 0.1–0.2 eV, they agree within $\approx$0.5 pK_a units for the acidity changes upon excitation. The higher-order corrections improve the correlation between the computed and the experimental values for ΔpK_a^*.

For the oxygen-based photoacids the estimated EC-RISM-CCSDR(3) and EC-RISM-CC3 results for ΔpK_a^* agree with the experimental results obtained from absorption band maxima within mean absolute deviations of, respectively, 2.31 and 2.61 pK_a units. For N-heterocyclic photobases the respective mean absolute deviations are 1.70 and 1.83 pK_a units. Considering that an error of only 0.1 eV in the difference of excitation energies between acid and base forms leads to an error of 1.69 pK_a units in the acidity change upon excitation, a large fraction of the remaining deviations is most likely due to the limitations that arise from the assignment of the band maxima and their approximation by computed vertical excitation energies.

Author contributions

Ömer F. C. Tiska: conceptualization, methodology, validation, investigation, formal analysis, visualization, writing – original draft. Niklas Sülzner: conceptualization, methodology, validation, visualization, supervision, review & editing. Julia Haberhauer: software, validation, supervision, review & editing. Patrick Kibies: software, review & editing. Christof Hättig: conceptualization, methodology, software, supervision, project administration, resources, funding acquisition, data curation, review & editing. Stefan Kast: methodology, software, review & editing.

Conflicts of interest

There are no conflicts to declare.

Data availability

NTOs for parent compounds used to assign L_a and L_b states; tables with states used to compute ΔpK_a^*; excitation energies in vacuum with CC2, CCSD, CCSDR(3), and CC3; excitation energies in solution with COSMO-CC2 for the coupling schemes post-SCF and PTED (with n = 1 and n = 1.30); linear response and higher-order corrections; and a convergence study for the restricted virtual space approximation. See DOI: https://doi.org/10.1039/d5cp01694k

Data for this article, including structures, input files, and output files with the original data are available at Zenodo[94] at https://doi.org/10.5281/zenodo.15283523 and at RESOLVdata[95] at https://doi.org/10.17877/RESOLV-2025-MAA3KZFH. Data supporting this article has also been included as part of the SI.

Acknowledgements

We acknowledge financial support by the Deutsche Forschungsgemeinschaft (DFG, German Research Foundation) under Germany's Excellence Strategy-EXC 2033-390677874-RESOLV.

References

1 P.-T. Chou and K. M. Solntsev, *J. Phys. Chem. B*, 2015, **119**, 2089.
2 H. Kagel, M. Frohme and J. Glökler, *J. Cell. Biotechnol.*, 2018, **4**, 23–30.
3 H. T. Pham, J. Yoo, M. VandenBerg and M. A. Muyskens, *J. Fluoresc.*, 2020, **30**, 71–80.
4 J. V. Crivello and J. Ahn, *J. Polym. Sci., Part A: Polym. Chem.*, 2003, **41**, 2570–2587.
5 X. Zhang, W. Xi, C. Wang, M. Podgórski and C. N. Bowman, *ACS Macro Lett.*, 2016, **5**, 229–233.
6 D. B. Spry and M. D. Fayer, *J. Phys. Chem. B*, 2009, **113**, 10210–10221.
7 C. Lawler and M. D. Fayer, *J. Phys. Chem. B*, 2015, **119**, 6024–6034.
8 C. Hoberg, J. J. Talbot, J. Shee, T. Ockelmann, D. D. Mahanta, F. Novelli, M. Head-Gordon and M. Havenith, *Chem. Sci.*, 2023, **14**, 4048–4058.
9 K. Adamczyk, M. Prémont-Schwarz, D. Pines, E. Pines and E. T. J. Nibbering, *Science*, 2009, **326**, 1690–1694.
10 R. Gepshtein, P. Leiderman, D. Huppert, E. Project, E. Nachliel and M. Gutman, *J. Phys. Chem. B*, 2006, **110**, 26354–26364.
11 N. Sülzner, B. Geissler, A. Grandjean, G. Jung and P. Nuernberger, *ChemPhotoChem*, 2022, **6**, e202200041.
12 J. Knorr, N. Sülzner, B. Geissler, C. Spies, A. Grandjean, R. J. Kutta, G. Jung and P. Nuernberger, *Photochem. Photobiol. Sci.*, 2022, **21**, 2179–2192.
13 N. Sülzner, G. Jung and P. Nuernberger, *Chem. Sci.*, 2025, 1560–1596.
14 E. M. Santos, W. Sheng, R. Esmatpour Salmani, S. Tahmasebi Nick, A. Ghanbarpour, H. Gholami, C. Vasileiou, J. H. Geiger and B. Borhan, *J. Am. Chem. Soc.*, 2021, **143**, 15091–15102.
15 P. Leiderman, L. Genosar and D. Huppert, *J. Phys. Chem. A*, 2005, **109**, 5965–5977.
16 A. Yucknovsky, Y. Shlosberg, N. Adir and N. Amdursky, *Angew. Chem., Int. Ed.*, 2023, **62**, e202301541.
17 Y. Xie, S. Ilic, S. Skaro, V. Maslak and K. D. Glusac, *J. Phys. Chem. A*, 2017, **121**, 448–457.

18 J. Ryan Hunt, C. Tseng and J. M. Dawlaty, *Faraday Discuss.*, 2019, **216**, 252–268.
19 E. Pines, *UV-Visible spectra and photoacidity of Phenols, Naphthols and Pyrenols*, John Wiley & Sons, Ltd, 2003, ch. 7, pp. 491–527.
20 T. Förster, *Naturwissenschaften*, 1949, **36**, 186–187.
21 T. Förster, *Z. Elektrochem. Angew. Phys. Chem.*, 1950, **54**, 42–46.
22 L. M. Tolbert and K. M. Solntsev, *Acc. Chem. Res.*, 2002, **35**, 19–27.
23 J. Ditkovich, T. Mukra, D. Pines, D. Huppert and E. Pines, *J. Phys. Chem. B*, 2015, **119**, 2690–2701.
24 E. Pines and D. Huppert, *J. Am. Chem. Soc.*, 1989, **111**, 4096–4097.
25 E. Pines, D. Huppert and N. Agmon, *J. Chem. Phys.*, 1988, **88**, 5620–5630.
26 N. Agmon, E. Pines and D. Huppert, *J. Chem. Phys.*, 1988, **88**, 5631–5638.
27 E. F. Caldin and V. Gold, *Proton-Transfer Reactions*, Springer, 2013.
28 N. Sülzner and C. Hättig, *J. Phys. Chem. A*, 2022, **126**, 5911–5923.
29 N. Sülzner and C. Hättig, *Phys. Chem. Chem. Phys.*, 2023, **25**, 11130–11144.
30 U. Raucci, M. G. Chiariello and N. Rega, *J. Chem. Theory Comput.*, 2020, **16**, 7033–7043.
31 A. Nitzan, *Chemical Dynamics in Condensed Phases: Relaxation, Transfer and Reactions in Condensed Molecular Systems*, Oxford University Press, 2006.
32 M. D. Driver, M. J. Williamson, J. L. Cook and C. A. Hunter, *Chem. Sci.*, 2020, **11**, 4456–4466.
33 B. Sharma, V. A. Tran, T. Pongratz, L. Galazzo, I. Zhurko, E. Bordignon, S. M. Kast, F. Neese and D. Marx, *J. Chem. Theory Comput.*, 2021, **17**, 6366–6386.
34 S. K. Khani, A. M. Khah and C. Hättig, *Phys. Chem. Chem. Phys.*, 2018, **20**, 16354–16363.
35 B. Mennucci, *Wiley Interdiscip. Rev.:Comput. Mol. Sci.*, 2012, **2**, 386–404.
36 B. Lunkenheimer and A. Köhn, *J. Chem. Theory Comput.*, 2013, **9**, 977–994.
37 A. Klamt and G. Schüürmann, *J. Chem. Soc., Perkin Trans. 2*, 1993, 799–805.
38 D. Chandler and H. C. Andersen, *J. Chem. Phys.*, 1972, **57**, 1930–1937.
39 F. Hirata, B. M. Pettitt and P. J. Rossky, *J. Chem. Phys.*, 1982, **77**, 509–520.
40 F. Hirata and P. J. Rossky, *Chem. Phys. Lett.*, 1981, **83**, 329–334.
41 D. Beglov and B. Roux, *J. Phys. Chem. B*, 1997, **101**, 7821–7826.
42 A. Kovalenko and F. Hirata, *Chem. Phys. Lett.*, 1998, **290**, 237–244.
43 J. Heil and S. M. Kast, *J. Chem. Phys.*, 2015, **142**, 114107.
44 S. M. Kast and T. Kloss, *J. Chem. Phys.*, 2008, **129**, 236101.
45 T. Kloss, J. Heil and S. M. Kast, *J. Phys. Chem. B*, 2008, **112**, 4337–4343.
46 S. Maste, B. Sharma, T. Pongratz, B. Grabe, W. Hiller, M. B. Erlach, W. Kremer, H. R. Kalbitzer, D. Marx and S. M. Kast, *Phys. Chem. Chem. Phys.*, 2024, **26**, 6386–6395.
47 V. A. Tran, M. Teucher, L. Galazzo, B. Sharma, T. Pongratz, S. M. Kast, D. Marx, E. Bordignon, A. Schnegg and F. Neese, *J. Phys. Chem. A*, 2023, **127**, 6447–6466.
48 N. Tielker, L. Eberlein, G. Hessler, K. F. Schmidt, S. Güssregen and S. M. Kast, *J. Comput.-Aided Mol. Des.*, 2021, **35**, 453–472.
49 T. Pongratz, P. Kibies, L. Eberlein, N. Tielker, C. Hölzl, S. Imoto, M. Beck Erlach, S. Kurrmann, P. H. Schummel, M. Hofmann, O. Reiser, R. Winter, W. Kremer, H. R. Kalbitzer, D. Marx, D. Horinek and S. M. Kast, *Biophys. Chem.*, 2020, **257**, 106258.
50 K. E. Ebbert, F. Sendzik, L. Neukirch, L. Eberlein, A. Platzek, P. Kibies, S. M. Kast and G. H. Clever, *Angew. Chem., Int. Ed.*, 2025, **64**, e202416076.
51 H. Sato, *Phys. Chem. Chem. Phys.*, 2013, **15**, 7450–7465.
52 K. Imamura, D. Yokogawa and H. Sato, *J. Chem. Phys.*, 2024, **160**, 050901.
53 A. Ghiami-Shomami and C. Hättig, *J. Comput. Chem.*, 2023, **44**, 1941–1955.
54 O. Christiansen, H. Koch and P. Jørgensen, *Chem. Phys. Lett.*, 1995, **243**, 409–418.
55 O. Christiansen, H. Koch and P. Jørgensen, *J. Chem. Phys.*, 1995, **103**, 7429–7441.
56 O. Christiansen, H. Koch and P. Jørgensen, *J. Chem. Phys.*, 1996, **105**, 1451–1459.
57 *TURBOMOLE V7.8 2023, a development of University of Karlsruhe and Forschungszentrum Karlsruhe GmbH, 1989–2007, TURBOMOLE GmbH, since 2007*, available from **https://www.turbomole.org**.
58 Y. J. Franzke, C. Holzer, J. H. Andersen, T. Begušić, F. Bruder, S. Coriani, F. Della Sala, E. Fabiano, D. A. Fedotov, S. Fürst, S. Gillhuber, R. Grotjahn, M. Kaupp, M. Kehry, M. Krstić, F. Mack, S. Majumdar, B. D. Nguyen, S. M. Parker, F. Pauly, A. Pausch, E. Perlt, G. S. Phun, A. Rajabi, D. Rappoport, B. Samal, T. Schrader, M. Sharma, E. Tapavicza, R. S. Treß, V. Voora, A. Wodyński, J. M. Yu, B. Zerulla, F. Furche, C. Hättig, M. Sierka, D. P. Tew and F. Weigend, *J. Chem. Theory Comput.*, 2023, **19**, 6859–6890.
59 S. Brode, H. Horn, M. Ehrig, D. Moldrup, J. E. Rice and R. Ahlrichs, *J. Comput. Chem.*, 1993, **14**, 1142–1148.
60 C. Hättig and F. Weigend, *J. Chem. Phys.*, 2000, **113**, 5154–5161.
61 A. Pausch, *J. Chem. Theory Comput.*, 2024, **20**, 3169–3183.
62 N. Tielker, L. Eberlein, S. Güssregen and S. M. Kast, *J. Comput.-Aided Mol. Des.*, 2018, **32**, 1151–1163.
63 P. J. Kibies, Dissertation, Technische Universität Dortmund, 2019.
64 D. A. Case, H. M. Aktulga, K. Belfon, I. Y. Ben-Shalom, J. T. Berryman, S. R. Brozell, D. S. Cerutti, T. E. Cheatham III, G. A. Cisneros, V. W. D. Cruzeiro, T. A. Darden, R. E. Duke, G. M. Giambasu, M. K. Gilson, H. Gohlke, A. W. Goetz, R. Harris, S. Izadi, S. A. Izmailov, Z. Jin, K. Kasavajhala, M. C. Kaymak, E. King, A. Kovalenko, T. Kurtzman, T.-F. Lee, S. LeGrand, P. Li, C. Lin, J. Liu, T. Luchko, R. Luo, V. Man, K. M. Merz, Y. Miao, G. Monard, H. D. Nguyen, H. Nguyen,

I. Omelyan, A. Onufriev, F. Pan, S. Pantano, R. Qi, D. R. Roe, A. Roitberg, C. Sagui, S. Schott-Verdugo, J. Shen, C. L. Simmerling, N. R. Skrynnikov, J. Smith, J. Swails, R. C. Walker, J. Wang, H. Wei, M. G. Wolf, X. Wu, Y. Xue, D. M. York, S. Zhao and P. A. Kollman, *Amber 2022 Reference Manual*, University of California, San Francisco, 2022.

65 J. Wang, R. M. Wolf, J. W. Caldwell, P. A. Kollman and D. A. Case, *J. Comput. Chem.*, 2004, **25**, 1157–1174.

66 J. Wang, W. Wang, P. A. Kollman and D. A. Case, *J. Mol. Graphics Modell.*, 2006, **25**, 247–260.

67 T. Schwabe, K. Sneskov, J. M. Haugaard Olsen, J. Kongsted, O. Christiansen and C. Hättig, *J. Chem. Theory Comput.*, 2012, **8**, 3274–3283.

68 A. Schäfer, C. Huber and R. Ahlrichs, *J. Chem. Phys.*, 1994, **100**, 5829–5835.

69 F. Weigend, M. Häser, H. Patzelt and R. Ahlrichs, *Chem. Phys. Lett.*, 1998, **294**, 143–152.

70 F. Weigend and R. Ahlrichs, *Phys. Chem. Chem. Phys.*, 2005, **7**, 3297–3305.

71 D. Rappoport and F. Furche, *J. Chem. Phys.*, 2010, **133**, 134105.

72 A. Hellweg and D. Rappoport, *Phys. Chem. Chem. Phys.*, 2015, **17**, 1010–1017.

73 C. Hättig and A. I. Pausch, *J. Phys. Chem. A*, 2025, **129**, 6155–6169.

74 J. M. Herbert, *Wiley Interdiscip. Rev.:Comput. Mol. Sci.*, 2021, **11**, e1519.

75 M. Reimann and M. Kaupp, *J. Phys. Chem. A*, 2020, **124**, 7439–7452.

76 J. L. Rosenberg and I. Brinn, *J. Phys. Chem.*, 1972, **76**, 3558–3562.

77 M. Prémont-Schwarz, T. Barak, D. Pines, E. T. J. Nibbering and E. Pines, *J. Phys. Chem. B*, 2013, **117**, 4594–4603.

78 L. M. Tolbert and J. E. Haubrich, *J. Am. Chem. Soc.*, 1990, **112**, 8163–8165.

79 E. L. Wehry and L. B. Rogers, *J. Am. Chem. Soc.*, 1965, **87**, 4234–4238.

80 S. G. Schulman, W. R. Vincent and W. J. M. Underberg, *J. Phys. Chem.*, 1981, **85**, 4068–4071.

81 L. Pinto da Silva, R. Simkovitch, D. Huppert and J. C. G. Esteves da Silva, *J. Photochem. Photobiol., A*, 2017, **338**, 23–36.

82 R. Simkovitch, L. Pinto da Silva, J. C. G. Esteves da Silva and D. Huppert, *J. Phys. Chem. B*, 2016, **120**, 10297–10310.

83 J. R. Platt, *J. Chem. Phys.*, 1949, **17**, 484–495.

84 F. J. Avila Ferrer, J. Cerezo, E. Stendardo, R. Improta and F. Santoro, *J. Chem. Theory Comput.*, 2013, **9**, 2072–2082.

85 S. Bai, R. Mansour, L. Stojanović, J. M. Toldo and M. Barbatti, *J. Mol. Model.*, 2020, **26**, 107.

86 S. P. A. Sauer, M. Schreiber, M. R. Silva-Junior and W. Thiel, *J. Chem. Theory Comput.*, 2009, **5**, 555–564.

87 P.-F. Loos, M. Comin, X. Blase and D. Jacquemin, *J. Chem. Theory Comput.*, 2021, **17**, 3666–3686.

88 S. Tsuru, B. Sharma, C. Hättig and D. Marx, *Angew. Chem., Int. Ed.*, 2025, **64**, e202416058.

89 A. Weller, *Z. Elektrochem., Ber. Bunsenges. Phys. Chem.*, 1957, **61**, 956–961.

90 E. W. Driscoll, PhD thesis, University of Southern California, 2017.

91 S. G. Schulman, R. M. Threatte, A. C. Capomacchia and W. Larry Paul, *J. Pharm. Sci.*, 1974, **63**, 876–880.

92 R. Send, V. R. I. Kaila and D. Sundholm, *J. Chem. Phys.*, 2011, **134**, 214114.

93 E. W. Driscoll, J. R. Hunt and J. M. Dawlaty, *J. Phys. Chem. Lett.*, 2016, **7**, 2093–2099.

94 Ö. Tiska, N. Sülzner, J. Haberhauer, P. J. Kibies, S. M. Kast and C. Hättig, *Raw data for: "Comparison of the solvation models COSMO and EC-RISM for the prediction of photoacidity in aqueous solution"*, 2025, DOI: **10.5281/zenodo.15283523**.

95 Ö. Tiska, N. Sülzner, J. Haberhauer, P. J. Kibies, S. M. Kast and C. Hättig, *Replication Data for: "Comparison of the solvation models COSMO and EC-RISM for the prediction of photoacidity in aqueous solution"*, 2025, DOI: **10.17877/RESOLV-2025-MAA3KZFH**.